CrossMark

ORIGINAL PAPER

Land-cover classification and analysis of change using machine-learning classifiers and multi-temporal remote sensing imagery

Hamidreza Keshtkar[1,2] · Winfried Voigt[1] · Esmaeil Alizadeh[2]

Abstract Frequent human activity and rapid urbanization have led to an assortment of environmental issues. Monitoring land-cover change is critical to efficient environmental management and urban planning. The current study had two objectives. The first was to compare pixel-based random forest (RF) and decision tree (DT) classifier methods and a support vector machine (SVM) algorithm both in pixel-based and object-based approaches for classification of land-cover in a heterogeneous landscape for 2010. The second was to examine spatio-temporal land-cover change over the last two decades (1990–2010) using Landsat data. This study found that the object-based SVM classifier is the most accurate with an overall classification accuracy of 93.54% and a kappa value of 0.88. A post-classification change detection algorithm was used to determine the trend of change between land-cover classes. The most significant change from 1990 to 2010 was caused by the expansion of built-up areas. In addition to the net changes, the rate of annual change for each phenomenon was calculated to obtain a better understanding of the process of change. Between 1990 and 2010, an average of 4.53% of lands turned to the built-up annually and there was an annual decrease of about 0.81% in natural land. If the current trend of change continues, regardless of the actions of sustainable development, drastic declines in natural areas will ensue. The results of this study can be a valuable baseline for land-cover managers in the region to better understand the current situation and adopt appropriate strategies for management of land-cover.

Keywords Decision tree · Land-cover · Object-based · Random forest · Support vector machines

Introduction

Land-cover is a key variable in both space and time with which to adjust parameters (e.g., exchange of carbon, water and energy) within and between earth systems (Brown de Colstoun and Walthall 2006). Change in land-cover is an important variable when assessing global changes that affect environmental systems (Loveland and Belward 1997). Recently, issues related to land-cover changes have attracted interest of those who model spatial and temporal patterns of land conversion to those who want to understand the causes and influences of land-cover change (Keshtkar and Voigt 2016b; Wu et al., 2008).

In general, intense human activity has increased construction and agricultural lands and has led to destruction of forests, meadows and other natural resources (Lambin and Geist 2003; Lawrence et al., 2012). Previous studies have indicated that anthropogenic activities associated with construction pollute the atmosphere, water, and soil (Kang et al., 2010; Li et al., 2009). The destruction of forests and meadows contributes to the loss of biodiversity, releases carbon into the atmosphere, and changes the surface albedo, which affects climate change (Foley et al., 2005; Hua and Chen 2013). Therefore, detailed and timely information about land-cover is essential for land change monitoring, management of ecosystems, and urban planning.

Previous researches have shown that some topographic factors (such as elevation and slope) influence the microclimatic conditions of a region (Freitas et al., 2010; Zhao et al., 2014).

✉ Hamidreza Keshtkar
  Hkeshtkar97@yahoo.com

[1] Institute of Ecology, Friedrich Schiller University, 07743 Jena, Germany

[2] College of Natural Resources, University of Tehran, Tehran, Iran

🍂 Springer

These topographic factors influence moisture, temperature, and solar radiation (Oke, 1987) and indirectly control the spatial patterns of plant species and land-cover types (Shrestha and Zinck, 2001; Deng et al., 2007). Moreover, topography is a major factor influencing the type of human activity that is influential in shaping landscape patterns. In other words, with the implementation of conservation measures, human choices regarding land-cover have changed greatly due to the impact of topographic factors (Chen et al., 2001; Fu et al., 2006). A built-up area tends begin in a flat area with good traffic conditions and a water supply. Therefore, analysis of the relationship between land-cover and topographic factors can guide managers for future land management and vegetation restoration.

Although there are several techniques that can be applied to analysis and presentation of resource data, but geographic information system (GIS) and remote sensing (RS) techniques are recognized as powerful tools and are widely used for the investigation of spatiotemporal dynamics of land-cover (Keshtkar and Voigt 2016a; Zhao et al. 2014). The availability of data in appropriate intervals and high/medium resolution satellite images are useful for both visual and quantitative assessments of land-cover dynamics over time (Keshtkar and Voigt 2016a). On the other hand, analysis and representation of such data can be considerably facilitated through the use of GIS techniques (Long et al. 2008).

Classification of satellite images is a common method for extracting information related to land-cover patterns and change. Several image classifier techniques have been developed, a comprehensive review of which can be found in Lu and Weng (2007). Selection of appropriate classification methods and imagery depends on the planned applicability of the final product. Land-cover classification by satellite images can be based on pixels or objects. While analysis based on pixels has been the dominant approach in the classification of remote sensing images, object-based image analysis has become more common in recent years (Blaschke 2010). Pixel-based methods use only spectral information to classify images, while object-based methods segment images into homogeneous regions (image segments) before classification and can use non-spectral information in the segmented images together with spectral information (e.g., mean, standard deviation) for classification (Johnson, 2013; Myint et al., 2011). Although some studies have compared thematic mapping accuracy produced using different classification algorithms, conflicting results have been obtained. For example, Adam et al. (2014) and Rodriguez-Galiano and Chica-Rivas (2012) reported that the random forest (RF) model achieved higher classification accuracies than the support vector machines (SVM) model. Conversely, Pal and Mather (2005) found that both RF and SVM classifiers produced similar classification accuracies. Also, Duro et al. (2012b), and Gislason et al. (2006) reported that the RF model achieved higher classification accuracies than the decision tree (DT)

model. While, Otukei and Blaschke (2010) discovered that DT generally achieved better classifications than those obtained using SVM. Therefore, more research is required in this area (especially for preparation of land-cover maps) to ascertain the superiority of one method or group of methods over others.

This study focuses on comparing various machine learning algorithms, i.e., RF (Breiman 2001; Ghimire et al. 2010), DT (Szantoi et al. 2015; Quinlan 1987), SVM (Szantoi et al. 2013; Vapnik 1995), and object-based support vector machines (OSVM, Duro et al. 2012b), to classifying Landsat image 2010. Furthermore land-cover maps of 1990 to 2010 produced using multi-temporal Landsat images (TM and ETM+) and the best classifier method. For this purpose, multispectral images of the study area over a period of two decades have been chosen to indicate the changes in land-cover phenomena. Our specific objectives were to (1) compare pixel-based and object-based classification methods for land-cover mapping, (2) identify the land-cover dynamics in the study area during the periods from 1990 to 2000, and 2000 to 2010 by using multi-temporal remotely sensed data and GIS, and (3) analyze the relationship between land-cover and topographic factors.

Materials and methods

Study area

The study area is located in central Germany and covers 6900 km^2 (Fig. 1). Elevation ranges from 114 to 982 m.a.s.l, with higher elevations concentrated in the Grosser Beerberg Mountain located in the Thuringian Forest. The predominant climate is of the continental type with an average annual rainfall of 604 mm and an average annual air temperature of 8.6 °C (based on monthly recording data of 18 stations, in Free State of Thuringia from 1960 to 1990). The soil parent material is mainly calcareous. The land-cover maps presented five classes: forest, built-up area, grassland, farmland, and water bodies (lakes, rivers, ponds, and reservoirs).

Landsat image collection and pre-processing

In this study, temporal coverage Landsat TM and ETM+ images from 1990 to 2010 with a standard spatial resolution of 30 × 30 m were obtained from the US Geological Survey (USGS) archive (http://earthexplorer.usgs.gov/). The study area is located into a southern and a northern Landsat image (path 194, rows 24 and 25), which were mosaicked into a single scene. Since Landsat ETM+ images from 2003 and beyond have high rates of no data values, images from 2010 were collected from Landsat TM. Image registration was performed by selecting an appropriate number of well-

Fig. 1 Location and elevation
model of study area
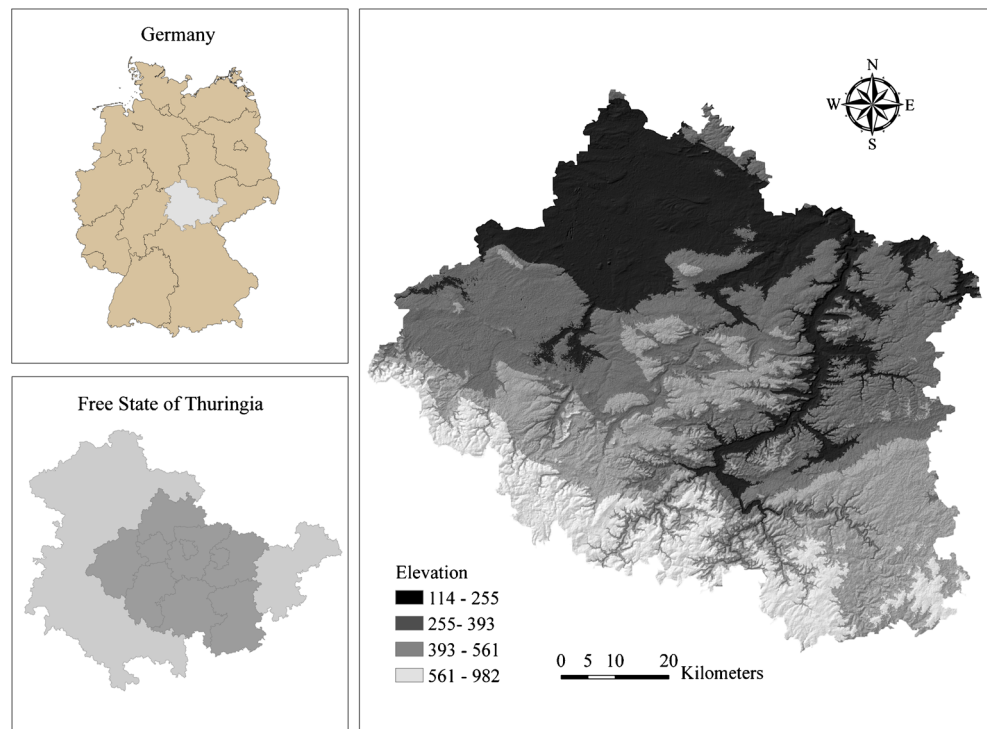
recognized ground control points (i.e., road intersections). A
second-order polynomial transformation was used to hold
down the root-mean-square error (RMSE). Eventually, images
with an error lower than a half-pixel (about 15 m) were regis-
tered. Moreover, the PCI Geomatica ATCOR model was used
for atmospheric correction (Geomatica 2013). Atmospheric
and terrain effects were removed to determine the true ground
reflectance of the Earth's surface. This model requires infor-
mation, some of which is available in the metadata file, in-
cluding date and time of data acquisition, sensor type, coordi-
nation of the image center, and atmospheric definition area.
Atmospheric definition area was set up as "rural" area and
atmospheric condition was determined as "mid-latitude sum-
mer."

Image classification

Images classification is one of the most important processes in
capturing detailed land-cover information. The model used in
this study operates in two stages. At the first stage, we com-
pared several classifiers that are considered to be suitable for
land-cover image classification. Training samples were select-
ed for training process before classification. After the selection
of training samples, different classification algorithms were
used to create the classified maps from Landsat 2010 image.
Then, the accuracy of classified maps was compared not only
by visual observation but also by statistical methods (Overall
accuracy and Kappa coefficient). The second stage involved
classifying all images (1990, 2000, and 2010) using the best

classification algorithm identified in the first stage and had a
process similar to that of first stage. Ultimately, all classified
maps undergo an accuracy evaluation.

Collection of training data

In this study, five land-cover categories (Built-up area, Forest
land, Framland, Grassland, Water bodies) have been deter-
mined with visual interpretation and analysis of the satellite
images. We gathered ground truth data (training and valida-
tion data) based on Quickbird images available in Google
Earth (http://earth.google.com). The geo-positional accuracy
of the Quicbird images was assessed by overlaying road and
topographic maps. This showed that the images were compa-
rable to that of the georeferenced Landsat images. For whole
of study area, a sample of ground truth points randomly col-
lected within the area covered by high-resolution Quickbird
images, overlaid selected points on the Quickbird images, and
then grouped these points to appropriate classes based on vi-
sual interpretation. A point was assumed as an especial class if
land-cover patches included at least one pixel. Based on visual
interpretation of the Landsat images, the training sites were
carefully determined and restricted to homogeneous regions
where class membership was permanent from 1990 to 2010.
We checked the separability of the training samples by
Jeffries-Matusita distance measure and optimized the sample
dataset until we achieved maximum stable accuracy. This op-
timizing task was carried out by removing training samples
that may have been sources of error or collecting new samples

to obviously misclassified categories. Finally, we used a sample of 1374 points were mapped from Quickbird images. We split all ground truth points into training (85%) and evaluation (15%) data.

Pixel-based image classification

Pixel-based image classification approaches either automatically allocate all the pixels in an image to land-cover types or classify them thematically pixel by pixel. In this study, three different pixel-based machine learning classifiers were applied on each data set, namely (1) random forest, (2) decision tree, and (3) support vector machines.

Decision tree

Decision tree (DT) is a non-parametric classification method which can deal with various types of datasets containing categorical variables. DT represents a set of constraints or conditions that are hierarchically organized and is composed of one root node (containing all data), a number of internal nodes (splits), and a set of terminal nodes (leaves). Each node in a decision tree has only one parent node and two or more descendent nodes (Breiman et al. 1984).

This model was run in R software (R Core Team, 2013) using the rpart package (Therneau and Atkinson 1997) which uses the Classification and Regression Tree algorithm (CART; Breiman et al., 1984). In this study, "information gain" measure was considered for deciding between alternative splits. The rpart package has two main parameters to be adjusted: The minimum number of observations in a node (minsplit), and maximum depth of tree (maxdepth). Although complex trees are more expressive and potentially allowing higher accuracy, but they do not generalize the data well and are more likely to overfit. Pruning the model by setting the minimum number of observations in a node or setting the maximum depth of the tree can avoid this problem. Therefore, we tried to examine several decision trees to achieve a strong model.

Random forests

RF is a nonparametric algorithm which is considered as an improved version of CART algorithm. RF method has two key parameters that must be adjusted: the number of tree (ntree) and the number of input variables (mtry). These two parameters must be optimized to improve the classification accuracy (Breiman 2001).

The splitting criterion used in this study was the Gini coefficient, and the stop criteria to stop splitting, i.e., the minimum number of samples in a node and the minimum impurity in a node were set 1 and 0, respectively, in

which values the decision trees will be full grown. We used a grid-search approach based on the OOB estimate of error to figure out the optimal combination for ntree and mtry parameters (Tian et al. 2009). Finally, the optimized parameters were entered into ImageRF in the EnMAP-Box to classify satellite image (Waske et al. 2012).

Support vector machines

A support vector machine (SVM) is a discriminative method that classifies data according to the statistical learning theory (Vapnik 1995). In this study, SVM was implemented using the radial basis function (RBF) kernel. The SVM implementation of ENVI 4.8 software (ITT Visual Solutions Inc., http://www.ittvis.com/) has four parameters to be adjusted: the kernel width "gamma (γ)," the penalty parameter (C), the number of pyramid levels to use, and the classification probability threshold value. Classification probability threshold is an important value for the SVM classifier since all rule probabilities less than this threshold are unclassified. We set zero value for this threshold that means all pixels had to be classified into one category. Also, we set zero value for the pyramid parameter, which force the model to processes the image at full resolution. By default, the inverse of the number of bands is set for the value of gamma. Studies have shown that the best combination of γ and C depends on the training data and cannot be known by default (Kuemmerle et al. 2009).

Object-based image classification

The image segmentation technique used consists of two key steps: (1) edge-based segmentation and (2) full lambda schedule merging. This procedure begins with multiscale edge-based segmentation that divides the images into image objects with similar spatial, spectral and textural characteristics. Over-segmentation and under-segmentation errors can occur in image segmentation (Kampouraki et al. 2008; Möller et al. 2007). A low segmentation level generally results in many small segments which bring about over-segmentation. On the contrary, a high segmentation level results in a few large segments that accord with different land-cover classes. Hence, a precise analysis appears necessary when choosing a segmentation scale (Liu and Xia 2010). Preventing formation of over-segmented statements, which can be a very difficult task, is one of fundamental phases in this process. The full lambda schedule model was used to solve over-segmentation problem; hence, segmentation is used in the integration stage where all adjacent segmentations, given their range and location features, are

integrated (Robinson et al. 2002). Merging continues if the algorithm catches a pair of adjacent regions, i and j, such that merging cost, ti,j is less than a described threshold lambda value, of 0 to 100. The full lambda schedule algorithm is estimated as,

$$t_{i,j} = \frac{\frac{|O_i| \times |O_j|}{|O_i| + |O_j|} \times \|u_i - u_j\|^2}{\text{length}(\partial(O_i, O_j))}$$

where O_i is region i of the image, $|O_i|$ denotes the area of region i, u_i is the average value in region i, u_j is the average value in region j, $\|u_i - u_j\|$ is the Euclidean distance between the spectral values of regions i and j, and length $(\partial(O_i, O_j))$ denotes the length of the common boundary of O_i and O_j.

We classified several image segmentations of different scales to identify the one with the highest overall accuracy. This trial-and-error approach is often utilized in object-based classifications (e.g., Dingle Robertson and King 2011; Duro et al. 2012b; Myint et al. 2011). Following the image segmentation process, object features were selected for use in the object-based classification.

Selecting object features for use in object-based classification can be based on user experience and previous studies (e.g., Duro et al. 2012a; Pu et al. 2011; Yu et al. 2006) or a feature selection method can be used prior to final classification (e.g., Qian et al. 2014; Van Coillie et al. 2007). In this study, the inclusion of object features was based on our knowledge and previous studies. Consequently, we selected out 16 object features. These 16 features included 12 features calculated based on the six multispectral bands, which is mean value and standard deviation of these bands. In addition, we chose intensity, texture-variance, texture-mean, and NDVI (Normalized Difference Vegetation Index) for classifications (Table 1). Finally, for executing SVM classification method, we selected training samples for each land-cover type based on the previously segmented and merged objects. All these processes have been done in ENVI ZOOM (Version 4.8) software (ITT Visual Solutions Inc., http://www.ittvis.com/).

Accuracy assessment

Accuracy assessment was based on the calculation of the overall accuracy, user's accuracy, producer's accuracy, and the Kappa index. We also used McNemar test to assess the statistical significance of superiority of each classification algorithm over another. This test is based on a chi-square (χ^2) statistics, computed from two error matrices and given as,

$$\chi^2 = \frac{(f_{12} - f_{21})^2}{f_{12} + f_{21}}$$

where $f12$ denotes the number of cases that are wrongly classified by classifier one but correctly classified by classifier two, and $f21$ denotes the number of cases that are correctly classified by classifier one but wrongly classified by classifier two (Manandhar et al. 2009).

Analyzing land-cover change

We calculated the net changes and annual changes in the land-cover within the study area to compare the status of this factor at different time periods. The net changes were obtained by pixel based post-classification change detection algorithm. The post-classification change detection method not only maps the changes magnitude, but also determines the trend of changes (from-to) between land-cover classes (Yuan et al. 2005). Net change was calculated as the difference in land-cover (in ha) between 1990 and 2010, whereas annual change rates (ACR) were calculated for each time period j as:

$$ACR_j = [(SC_j / CPB_j) \times 100]/Y$$

where SC is the sum of changes in time period j, CPB is the cover of each phenomenon at the beginning of time period j, and Y donates the number of years between image A and image B.

To assess whether land-cover change varied with altitude and slope, we classified the digital elevation model (DEM) into four classes (class 1 (<255 m), class 2 (255–393 m), class

Table 1 Image object features used in object-based classification

Object features	Description
Spectral-mean	Mean value of the pixels comprising the region in a specific band
Spectral-STD	Standard deviation value of the pixels comprising the region in a specific band
Texture-mean	Average value of the pixels comprising the region inside the kernel
Texture-variance	Average variance of the pixels comprising the region inside the kernel
Intensity	Intensity using the *spectral-mean* attributes and is measured in floating-point values from 0 to 1.
NDVI	Normalized Difference Vegetation Index: (band4 − band3)/(band4 + band3)

3 (393–561 m), and class 4 (>561 m)) using Jenks natural breaks classification method and calculated percentage of net land change for each class. Likewise, we summarized net land-cover changes for three slope classes: gentle (<5°), moderate (5–10°), and steep (>10°).

Results

Class separability

The six reflective bands of the Landsat images were used as the reference basis for the calculation of the separability index of the collected spectra from the training sites indicating the different classes. Table 2 shows pairwise spectral separability values of different classes of training samples for 2010 image classification. Values range from 0 to 2. The closer to 2, the more separable training samples have been selected. Values more than 1.8 indicate that class pairs have good separability, while values less than 1 represent that the class pairs must be joint into one class (Petropoulos et al. 2010). Observing the values shown in Table 2, most of the class pairs are well separated from each other with values more than 1.8. Farmland and grassland have comparatively lower value (1.65); and class separability value of pair of farmland and built-up area (1.63) is also relatively lower than other pairs. Thus, no class has to be combined into others because all values are greater than 1. The selected training samples are satisfactory to be used for classification.

Tuning of machine learning algorithm parameters

For the DT classifier, the minsplit was set to 5 and examined a set of maxdepth from 2 to 7, which yielded a total of 6 classified images. No minsplit value of less than 5 was selected because setting minsplit to a very small value runs the risk of overfitting. The results showed that the highest overall classification accuracy (percentage of correctly classified samples) was achieved at a maximum depth value of 6. The structure of the final decision tree is shown in Fig. 2.

Table 2 Class separability of training samples of 2010 image

Separability values	Forest	Water	Farmland	Grassland	Built-up area
Forest	–	1.89	1.92	1.97	1.96
Water	1.89	–	1.99	1.99	1.99
Farmland	1.92	1.99	–	1.65	1.63
Grassland	1.97	1.99	1.65	–	1.83
Built-up area	1.96	1.99	1.63	1.83	–

To optimize the ntree and mtry parameters for the RF classification model, mtry settings from 1 to 6 were examined. The range for the ntree parameter was 100 to 1000 at intervals of 100, which resulted in 60 classifications. The results indicated that the ntree setting of 900 combined with a mtry setting of 2 produced the lowest OOB error rate (4.54%). The highest OOB error rate (5.81%) was produced by a combination of a mtry setting of 1 with a ntree setting of 100 (Fig. 3b).

For SVM-based classifications, a grid-search approach was used to find the optimal combination for γ and C parameters. Therefore, the gamma was adjusted by considering a nested cross-validation process, where γ (10^{-3}, 10^{-2}, 10^{-1}, 1, 10, 10^{2}, 10^{3}). Also, we set the C parameter by considering a nested cross-validation with C (10^{-2}, 10^{-1}, 1, 10, 10^{2}, 10^{3}). Results from the grid search indicated that the γ value of 1 combined with a C value of 10 produced the highest accuracy for the SVM-based classifications (pixel and object-based methods) (Fig. 3a).

Also, for object-based classifier, an iterative trial-and-error approach was used to identify the best image segmentation scale based on the highest overall accuracy. Results show that the scale value of 50 without merging to reduce the number of segments produced the highest accuracy for the object-based classification method (Table 3).

Accuracy assessment and statistical comparisons

Classification was conducted on 2010 image using four different machine learning classifiers, which were DT, RF, SVM, and OSVM. The classification maps are shown in Fig. 4. Analyzing the classification maps from Fig. 4a–d visually, indicate that all classifiers can generate useful land-cover maps and produce consistent classification results.

In addition to visually observing the classification maps, the accuracy of the classification maps was assessed to quantitatively compare the performance of these classifiers. The classification accuracy statistics are summarized in Table 4. The results show that classification using OSVM provided the highest overall accuracy (93.54%) and Kappa coefficient (0.88). DT generated the least accurate classification map with 86.36% overall accuracy and a Kappa coefficient of 0.76. Classification maps generated by RF and SVM showed much higher overall accuracy (90.28 and 90.93%, respectively) than DT, but the values were slightly lower than for OSVM.

For the OSVM, the classes with the highest producer's accuracy were those of water (96.58%), forests (96.31%), and farmland (96.13%) followed by built-up areas (94.06%). The lowest producer's accuracy was obtained for grassland (63.36%). User's accuracy was higher for water bodies (98.61%), forests (96.71%), and farmland
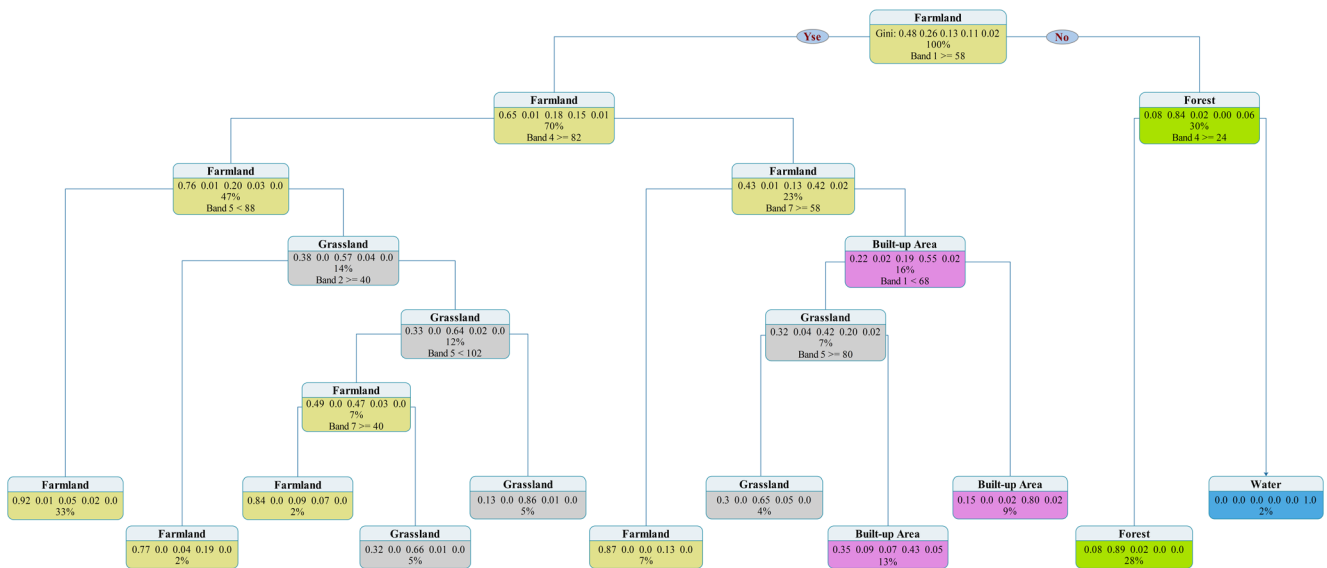
Fig. 2 Structure of the decision tree

(94.57%), followed by grassland (87.74%). The lowest user's accuracy was found for the built-up areas (78.44%). All classes were easily separable by all classifier algorithms applied. SVM and OSVM classifiers for grassland showed relatively poor or indistinct producer's and user's accuracy. For RF classification, this was for grassland and built-up areas and for DT, it was water, grassland, and built-up areas.

Also, we used the McNemar test to figure out whether a statistically significant difference exists between different machine learning algorithm. The McNemar test indicated that the observed difference between pixel-based image classifications was not statistically significant ($p > 0.05$). For pixel-based classifier methods and object-based classifier, a

statistically significant difference ($p < 0.05$) between DT and OSVM algorithms ($p = 0.004$) was observed, while RF and SVM algorithms did not show significant difference with OSVM method ($p > 0.05$).

Analysis of land-cover change

Object-based classification (i.e., OSVM algorithm) was performed on three Landsat images of 1990, 2000 and 2010. Accuracy assessment result of each classification map is summarized in Table 5. By counting the number of pixels of each phenomena for each year, land-cover coverage information can be obtained, which is shown as Fig. 5.
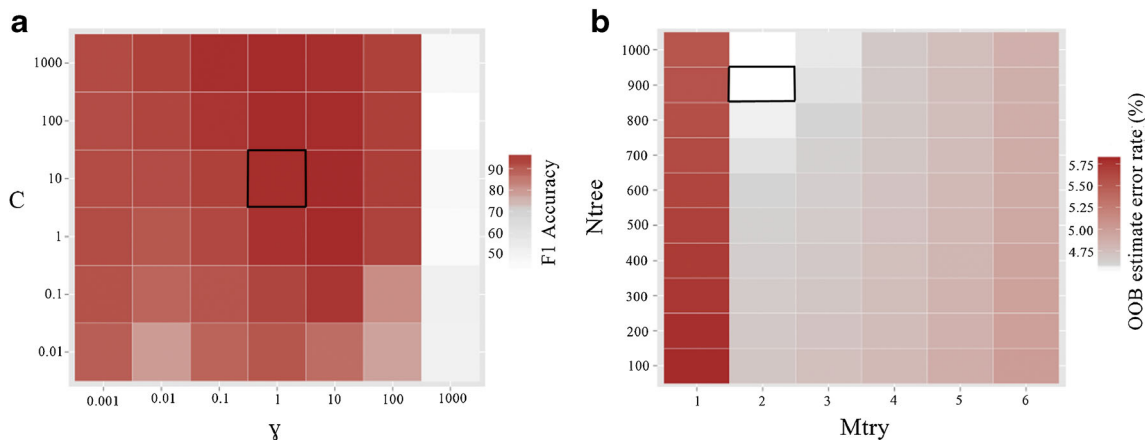

Fig. 3 Heat maps resulted from grid search procedure. **a** Optimization of the SVM parameters (C and γ). The F1 measure was used to determine the best accuracy for the different combinations ($n = 42$) of parameters. **b**

Optimization of the RF parameters (mtry and ntree). The OOB sample was used to determine the error rate for the different combinations ($n = 60$) of parameters

Table 3 The classification result (overall accuracy) of values for image segmentation parameters used in the object-based method. Values in bracket are the kappa coefficient

Merge level	Scale level						
	20	30	40	50	60	70	80
0	93.35 (0.882)	93.35 (0.882)	93.35 (0.882)	93.54 (0.884)	92.09 (0.853)	83.56 (0.715)	67.92 (0.352)
20	93.20 (0.879)	93.20 (0.879)	93.20 (0.879)	93.35 (0.880)	91.80 (0.847)	83.51 (0.697)	67.99 (0.352)
40	92.77 (0.870)	92.77 (0.870)	92.77 (0.870)	92.55 (0.863)	91.63 (0.843)	83.01 (0.691)	66.63 (0.326)
60	90.36 (0.822)	90.36 (0.822)	90.36 (0.822)	90.34 (0.819)	91.46 (0.840)	81.27 (0.678)	65.93 (0.321)
80	89.02 (0.794)	89.13 (0.794)	89.15 (0.797)	89.61 (0.803)	88.83 (0.789)	80.64 (0.656)	66.09 (0.313)

According to the change detection results, the most significant change occurred from 1990 to 2010 is caused by the expansion of built-up area. Analysis of land-cover area changes indicate that during this time period, built-up areas increased from 2.8% to 5.5%. The built-up land was continuously increased, and the farmland, grassland and forest were

Forest
Water
Built-up
Farmland
Grassland

Kilometers
0   10   20   40
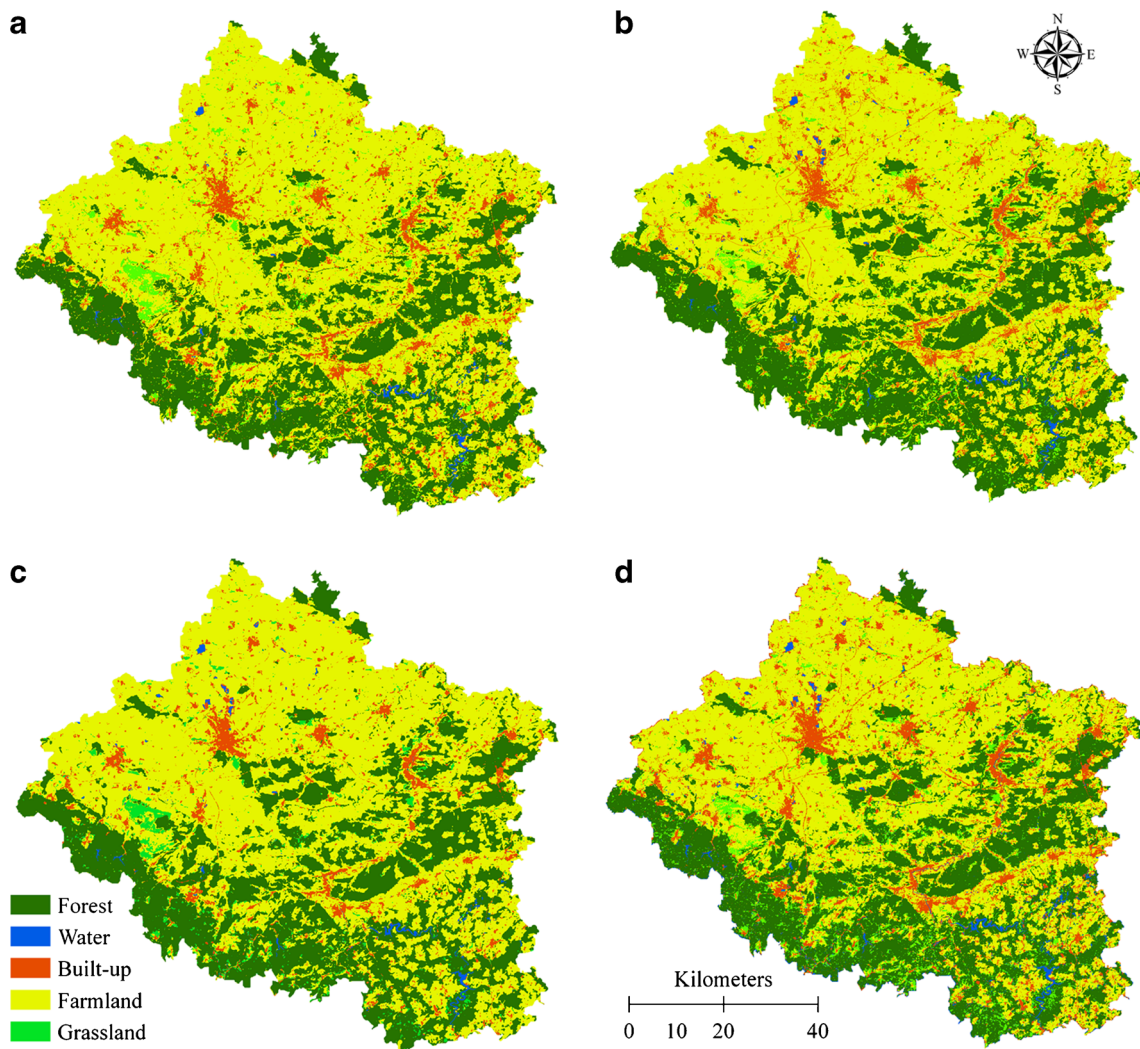
Fig. 4 Land-cover maps of 2010 generated by **a** DT, **b** RF, **c** SVM, and **d** OSVM classification algorithms

Table 4 Summary of mapping accuracy obtained by different classifiers to the Landsat TM 2010 image

	DT		RF		SVM		OSVM	
	OA (86.36)	K (0.76)	OA (90.28)	K (0.85)	OA (90.93)	K (0.86)	OA (93.54)	K (0.88)
Class	UA (%)	PA (%)	UA (%)	PA (%)	UA (%)	PA (%)	UA (%)	PA (%)
Forest	95.76	84.41	96.19	95.49	97.26	94.05	97.71	96.31
Water	99.17	56.70	99.00	93.86	99.20	94.07	99.61	96.58
Farmland	89.47	89.24	86.24	93.65	88.97	93.31	94.57	96.13
Grassland	66.39	81.53	83.54	61.06	80.77	56.33	87.74	63.36
Built-up	56.09	81.23	63.68	89.77	78.34	90.07	78.44	94.06

OA overall accuracy, *K* kappa coefficient, *UA* user's accuracy, *PA* producer's accuracy

continuously decreased. Grasslands decreased significantly from 4.89 to 4.02% during 1990–2010. During this period, forest area decreased from 32.38 to 32.26%. Also, the coverage of farmlands reduced from 59.21 to 57.58% in the same time. The area of water increased a little.

Figure 5 only illustrates the static state of each phenomenon in 1990, 2000, and 2010. Table 6 depicts the summarized specific "from-to" change information. This table represents the amount of change from one class detected in 1990 to another class detected in 2010. The diagonal values in table represent the area with no change. Forest and farmland are moderately stable classes that don't have significant change, keeping 91.23% and 94.53% unchanged respectively. About 5.04% of forest change to farmland and 2.54% change to grasslands. As for farmland, a small portion (2.94%) of the area changes to built-up area and another small portions, i.e., 1.69, 0.8, and 0.04%, changes to grassland, forest, and water bodies, respectively. Comparatively, grasslands experience the most dramatic change. Only about 56.35% of grasslands were kept unchanged. 19.76 and 16.3% of grasslands alter into farmland and forest, respectively.

Table 7 shows the ACR of land-cover classes for three time periods, 1990–2000, 2000–2010, and 1990–2010. This table

indicates that mean annual deforestation rates were three times higher in 1990–2000 compared to 2000–2010. The maximum rate of annual change in water bodies belonged to the years 1990–2000 and was about four times higher than the rate of the succeeding 10 years (2000–2010). Mean annual degradation rates of farmland and grassland in 1990–2000 were almost two times higher than the same rates in 2000–2010. Also, the results showed that the ACR of built-up area for 1990–2000 and 2000–2010 was 3.53 and 4.09%, respectively. Between the years 1990 and 2010, an annual average of about 4.53% of lands became built-up. Figure 6 illustrates the produced land-cover maps.

Land-cover changes in relation to topographic factors

The elevation distribution of each land-cover class is shown in Table 8. Elevation in the study area is mostly less than 400 m. The areas with an elevation of <255 m (class 1), 255–393 m (class 2), 393–561 m (class 3), and >561 m (class 4) accounted for 25.4, 36.5, 25.6, and 12.4% of the whole area, respectively.

The results show that more than 80% of class 1 and 60% of class 2 lands are allocated to farmland; forest, and farmland occupy approximately 47 and 42%, respectively, of class 3 lands; and more than 70% of class 4 land is covered by forest; only 20% of class 4 land is farmland. The mean elevation of each land-cover class is, in ascending order, built-up area (about 290 m) <farmland (about 310 m) <water bodies (about 350 m) <forest and grassland (over 430 m). During the years 1990–2010, changes in class 1 land reduced the area of farmland by 98.6 km^2 and increased built-up areas by 81.7 km^2. The most major change was related to the increase in built-up lands, which was as much as 60.3 km^2. The decrease of 38.5 km^2 in grassland reflected the greatest change in class 3 land. Forest land underwent the largest change with a loss of 16.4 km^2.

The results obtained from the division of the study area based on slope show that about 61% of the area under study has a slope below 5 degrees (4220.56 km^2), and over 70% of this slope category is farmland. More than 85% of built-up

Table 5 Summary of mapping accuracy obtained by object-based SVM classifier to the Landsat 1990, 2000, and 2010 images

	1990		2000		2010	
	OA (89.75)	K (0.84)	OA (92.36)	K (0.85)	OA (93.54)	K (0.88)
Class	UA (%)	PA (%)	UA (%)	PA (%)	UA (%)	PA (%)
Forest	97.35	94.23	97.14	96.51	96.71	96.31
Water	99.66	96.99	96.97	96.76	98.61	96.58
Farmland	77.39	92.87	91.87	97.64	94.57	96.13
Grassland	97.16	61.65	84.35	65.37	87.74	63.36
Built-up	86.93	89.28	79.46	93.56	78.44	94.06

OA overall accuracy, *K* kappa coefficient, *UA* user's accuracy, *PA* producer's accuracy
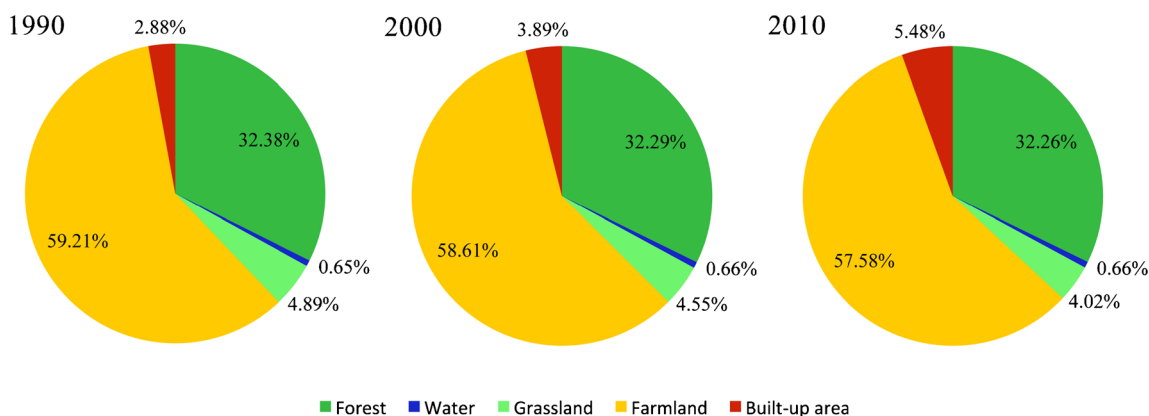
Fig. 5 Pie chart of land-cover coverage (%) from 1990 to 2010

areas occupy slopes below 5 degrees. Additionally, over 22% of the study area (1532.28 km^2) has a slope of 5–10 degrees. Forest and farmland cover about 46 and 44% of this slope gradient category, respectively. About 17% of the study area has a slope greater than 10 degrees (1146.56 km2), about 75% of which is covered by forest (Table 9). The mean slope gradients of built-up land and farmland are less than 3.3°, while those of forest, grassland, and water bodies are more than 5°.

Discussion and conclusion

This study compared various machine-learning algorithms (i.e., RF, DT, SVM, and OSVM) with classifying Landsat image 2010. Furthermore, land-cover maps of 1990, 2000, and 2010 were produced using multi-temporal Landsat images.

Land-cover classification

The results showed that SVM has the highest accuracy among pixel-based methods compared with two other methods (i.e., RF and DT) (Table 4), although the McNemar test did not

Table 6 Change detection classification matrix for 1990–2010 based on post-classification comparison to specify "from–to" transitions. The amount of changes is demonstrated by percentage (%). Italicized entries denote that there is no change in land-cover between two dates

	Class	1990				
		Forest	Water	Built-up	Farmland	Grassland
2010	Forest	*91.23*	15.98	2.20	0.80	16.30
	Water	0.35	*75.94*	0.88	0.04	0.57
	Built-up	0.84	3.64	*76.26*	2.94	7.03
	Farmland	5.04	3.25	18.88	*94.53*	19.76
	Grassland	2.54	1.19	1.79	1.69	*56.35*

show a significant difference in the performance of these three models ($p > 0.05$). It is noteworthy that both RF and SVM algorithms can obtain similar overall classification accuracies which are usually greater than those acquired using DT-based algorithms (Table 4). All in all, the classification results reported here are generally in agreement with results reported by some other authors such as Duro et al. (2012b), Gislason et al. (2006), and Pal and Mather (2005).

The high overall accuracy of the SVM classifier can be attributed to the ability of this method to optimally separate hyperplanes into classes for comparison with pixel-based methods (Licciardi et al., 2009) that may not be able to identify hyperplanes. SVMs also can generalize this optimal separating hyperplane to unseen samples with the minimum errors between all separating hyperplanes. This allows them to make the best class separation at the end of the classification. Additionally, SVMs attain their assessment directly from the training data in an appropriate space that is explained by a kernel function.

In this study, classifications created by either pixel-based or object-based image analysis produced to roughly similar and visually acceptable representations of the land-cover classes existing in the study area. The McNemar test showed that there is no statistical basis for preferring pixel-based to object-based classifiers. As expected, the object-based classifier approach (i.e., OSVM) in comparison to the pixel-based classifications obtained a more generalized visual appearance and more contiguous representation of land-cover, which possibly better shows how land-cover interpreters and analysts recognize the landscape (Stuckens et al. 2000).

One weakness of the pixel-based method is the "salt and pepper" effect (Fung et al., 2008). The restriction of this effect is not a problem in object-based methods. In the present study, relatively higher accuracy was achieved using a combination of segmentation and contextual information coming from image objects. The use of segmentation to collect pixels into objects helped to decrease the

Table 7 Distribution of land-cover classes (in Km²) and annual change rates (ACR) for 1990–2010

	Year			ACR in land-cover structure		
	1990	2000	2010	Δ%1990–2000	Δ%2000–2010	Δ%1990–2010
Forest	2234	2228.1	2225.5	−0.26	−0.12	−0.38
Water	44.6	45.3	45.5	1.57	0.44	2.02
Grassland	337.5	313.9	277.5	−6.99	−11.60	−17.78
Farmland	4084.9	4043.7	3972.7	−1.01	−1.76	−2.75
Built-up area	198.4	268.4	378.2	35.28	40.91	90.63

variability of the pixels and, thus, the salt and pepper effect. Class discrimination was higher using the object-based method than the pixel-based methods, as shown by the higher user accuracy for different classes (Table 4). Some researchers (e.g., Benz et al., 2004; Fung et al., 2008) have emphasized the advantages of object-based methods over pixel-based classifiers, which is consistent with the results of the present study. Although the accuracy of classification is important when selecting a classification method, choosing an image analysis approach is not always done based on accuracy (Duro et al., 2012a). In situations in which the statistical difference among the classification algorithms is low, the end-user may select these models by considering other factors. For example, being cost-free, user-friendly, and easily available might encourage the user to select a specific model.
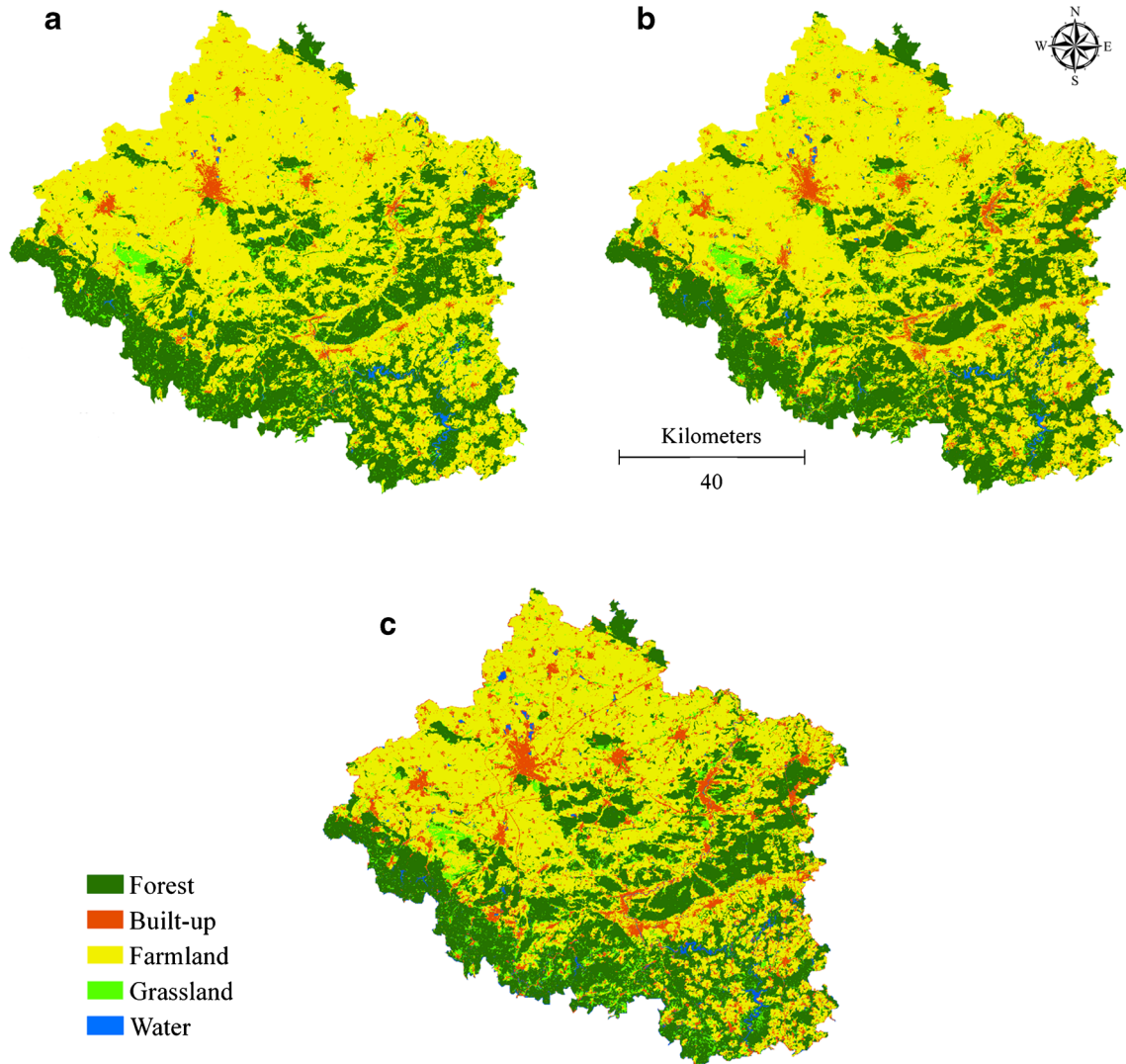
Fig. 6 Time series of detailed land-cover maps for **a** 1990, **b** 2000, and **c** 2010

Table 8 Land-cover changes in relation to elevation during 1990–2010

		Forest	Built-up	Farmland	Grassland	Water
Mean (m)	1990	475	277	306	434	350
	2010	472	295	310	430	340
	Changes	−3	18	4	−4	−10
1990 (km^2)	Class 1	81.3	105.2	1526.2	30.4	10.0
	Class 2	690.4	66.3	1642.6	108.1	14.2
	Class 3	837.5	22.0	750.2	138.4	19.3
	Class 4	624.8	4.8	165.9	60.7	1.2
2010 (km^2)	Class 1	79.9	186.9	1427.6	46.2	12.5
	Class 2	696.6	126.7	1609.8	76.0	12.6
	Class 3	840.6	54.9	753.9	99.9	18.0
	Class 4	608.3	9.7	181.4	55.5	2.4
Land-cover changes (km^2)	Class 1	−1.4	81.7	−98.6	15.8	2.5
	Class 2	6.1	60.3	−32.8	−32.1	−1.6
	Class 3	3.1	32.9	3.8	−38.5	−1.3
	Class 4	−16.4	5.0	15.4	−5.2	1.2

Land-cover change

This study shows that urbanization of land-cover in the past two decades has been rapid. This suggests that natural land affected by human activity are rapidly transforming and being damaged. Expansion of urban areas into agricultural and forest lands can decrease the effectiveness of rural areas as a buffer zone between forests and agricultural and urban land (DeFries et al. 2005). This can increase environmental impacts such as diversity loss (Haines-Young, 2009), deforestation (Keshtkar and Voigt, 2016a), land degradation (Bajocco et al. 2012), and landscape fragmentation (Keshtkar and Voigt, 2016b).

The main driving force for built-up area expansion would appear to be the implement of the urban development, termed "Critical Reconstruction," in the region since 1990 (Tölle 2010). The implementation of this policy caused open and empty areas around cities and many lands (i.e., agricultural lands) in the countryside to be converted quickly into industrial and urban areas after the year 1990 (Loeb 2006). Therefore, transition probability from other lands to built-up areas was extremely high in eastern regions (such as our study area) during these years. It highlights the fact that an increase in built-up area could be interpreted as a decrease in natural lands (nature land = total land area − (farmland area + built-up area); Lambin and Meyfroidt 2011). Degradation and loss of natural and semi-natural lands has become a profound concern which almost has affected the entire Western and Central Europe (CBD 2010; GBO3 2010; Poschlod et al. 2005; Riecken et al. 2008).

Our study clearly shows the high vulnerability of grasslands in the study area. The grasslands are decreasing in our study area, while previous studies warned that grassland

Table 9 Land-cover changes in relation to slope during 1990–2010

		Forest	Built-up	Farmland	Grassland	Water
Mean (degree)	1990	9	3	3	7	6
	2010	9	3	3	7	5
	Changes	0	0	0	0	−1
1990 (km^2)	<5°	681.9	168.5	3194.6	151.6	23.9
	5°–10°	679.9	26.4	713.4	101.8	10.8
	>10°	592.5	2.7	150.9	58.9	6.7
2010 (km^2)	<5°	686.5	325.5	3054.0	127.9	26.7
	5°–10°	681.9	38.6	728.8	72.3	10.6
	>10°	583.4	11.9	161.7	48.0	6.5
Land-cover changes (km^2)	<5°	4.6	157.0	−140.6	−23.6	2.7
	5°–10°	2.1	12.2	15.5	−29.5	−0.2
	>10°	−15.1	10.6	13.0	−6.8	−1.6

deterioration could have a significant impact on ecosystem services (i.e., the carbon cycle, regional economy and climate) (Angell and McClaran 2001; Le Houérou 1996; Wen et al. 2013). Despite the fact that grasslands are the habitat for more than 50% of vascular plant species in Central Europe (Lind et al. 2009), the European Topic Centre for Biological Diversity (ETC-BD) reports that grasslands are among the endangered habitats in the European regions and only 20% of them are in a favorable conditions (EU-COM 2009; Siehoff et al. 2011).

Post-classification change detection results showed that the destroyed forests had been primarily converted into farmland or grassland. Table 6 indicates that deforestation and reforestation are happening concurrently, but the speed and amount of deforestation is greater. Settel (1946) reported that after the World War II, timber exports from Germany were particularly heavy and forest areas dramatically decreased consequently. Changes in national and regional policies caused the rate of deforestation to decline (FAO 2011). The effect of this policy change is also visible in the results of the present study. The annual rate of deforestation in the second decade decreased significantly to one-third that of the first decade. All in all, forests have shown the fewest changes between the years 1990–2010 after water bodies. This reflects the greater stability of these regions than others in the study area.

In the present case study, most cultivated areas are located near urban areas, highlighting the potential competition for land between agricultural and urban uses. This is the reason for the decline between 1990 and 2010 in these lands (Table 7). Although the farmland area decreased due to development, this category still covered the largest land area. It is expected that land scarcity will cause more intensive use of agricultural land in the future (Ewert et al., 2006), although the decrease agricultural land can be compensated by a global food system (d'Amoura et al., 2016).

Land-cover change in relation to topography

The results show that as slope and altitude increased, forest areas also increased (Tables 8 and 9). Stretches of forest areas concentrated in the high lands create continuous habitat corridors which can be expected to have a significant effect on conserving biodiversity in the study area (Horskins et al. 2006). Unlike forest lands, however, the area covered by other phenomena decreased as slope increased. This is especially pronounced in the case of farmland and built-up areas. More than 75% of farmlands are located at a slope below 5 degrees, and only about 5% appear on slopes greater than 10 degrees. In particular, our analysis results confirmed that increased urbanization was not limited to the low, flat areas. Although built-up areas spread significantly in areas with a slope of less than 5 degrees from 1990 to 2010, the development of these lands has expanded into areas with higher slopes. The development of built-up areas and farmland has caused the destruction of natural lands, especially grasslands and forests, which have lost 7 and 15 km^2 of their area, respectively. Most grasslands were located at high altitudes, but their area decreased in the years 1990–2010 in all height classes (except class 1). Grassland in classes 2 and 3 has largely been replaced by built-up land. This may indicate that the development of built-up areas and their penetration into grassland is legally much easier than the penetration into forest or farmland; perhaps grasslands have the features necessary for urbanism. It should be noted that during the years 1990–2010, changes in land-cover occurred generally in areas with a slope of less than 5 degrees; that includes about 54% of total changes in these years. These results suggest that incorporating terrain characteristics and satellite images can be effective when developing conservation measures for cultivated land and natural areas.

The results indicate that effective measures for protecting agricultural land, grassland, and forests against urban development is critical, considering the rapid economic development that has recently taken place. Moreover, along with protective measures, regeneration of destroyed lands must also be considered. Environmental managers for implementation and monitoring of such processes and understanding spatial distributions and patterns of land-cover require refined base information such as more accurate land-cover classification maps (Keshtkar et al., 2013). Also, understanding how the topography influences land-cover diversity and distribution could help ecologists and environmental managers better manage wildlife habitat and thus promote ecosystem sustainability within the study area.

References

Adam E, Mutanga O, Abdel-Rahman EM, Ismail R (2014) Estimating standing biomass in papyrus (*Cyperus papyrus* L.) swamp: exploratory of in situ hyperspectral indices and random forest regression. Int J Remote Sens 35:693–714. doi:10.1080/01431161.2013.870676

Angell DL, McClaran MP (2001) Long-term influences of livestock management and a non-native grass on grass dynamics in the desert grassland. J Arid Environ 49:507–520. doi:10.1006/jare.2001.0811

Bajocco S, Angelis A, Perini L, Ferrara A, Salvati L (2012) The impact of land use/land cover changes on land degradation dynamics. A Mediterranean Case Study Environmental Management 49:980–989. doi:10.1007/s00267-012-9831-8

Benz UC, Hofmann P, Willhauck G, Lingenfelder I, Heynen M (2004) Multi-resolution, object-oriented fuzzy analysis of remote sensing data for GIS-ready information ISPRS. Journal of Photogrammetry and Remote Sensing 58:239–258. doi:10.1016/j.isprsjprs.2003.10.002

Blaschke T (2010) Object based image analysis for remote sensing ISPRS. Journal of Photogrammetry and Remote Sensing 65:2–16. doi:10.1016/j.isprsjprs.2009.06.004

Breiman L (2001) Random Forests. Machine Learning 45:5–32. doi:10.1023/A:1010933404324

Breiman L, Friedman J, Stone CJ, Olshen RA (1984) Classification and Regression Trees. Taylor & Francis

Brown de Colstoun EC, Walthall, CL (2006) Improving global scale land cover classifications with multidirectional POLDER data and a decision tree classifier. Remote Sens Environ 100(4):474–485

CBD (2010) Fourth national report under the convention on biological diversity (CBD)—Germany. http://www.cbd.int/reports/search/.

Chen L, Wang J, Fu B, Qiu Y (2001) Land-use change in a small catchment of northern loess plateau. China Agriculture, Ecosystems & Environment 86:163–172

d'Amoura CB et al (2016) Future urban land expansion and implications for global croplands. PNAS. doi:10.1073/pnas.1606036114

DeFries R, Hansen AJ, Newton AC, Hansen M (2005) Increasing solation of protected areas in tropical forests over the past twenty years. Ecol Appl 15(1):19–26

Deng Y, Chen X, Chuvieco E, Warner T, Wilson JP (2007) Multi-scale linkages between topographic attributes and vegetation indices in a mountainous landscape. Remote Sens Environ 111:122–134

Dingle Robertson L, King DJ (2011) Comparison of pixel- and object-based classification in land cover change mapping. Int J Remote Sens 32:1505–1529. doi:10.1080/01431160903571791

Duro DC, Franklin SE, Dubé MG (2012b) Multi-scale object-based image analysis and feature selection of multi-sensor earth observation imagery using random forests. Int J Remote Sens 33:4502–4526. doi:10.1080/01431161.2011.649864

Duro DC, Franklin SE, Dubé MG (2012a) A comparison of pixel-based and object-based image analysis with selected machine learning algorithms for the classification of agricultural landscapes using SPOT-5 HRG imagery. Remote Sens Environ 118:259–272. doi:10.1016/j.rse.2011.11.020

EU-COM (2009) Composite report on the conservation status of habitat types and species as required under article 17 of habitats directive. Report from the Commission to the Council and the European Parliament, Brussles

Ewert F, Rounsevell M, Reginster I, Metzger M, Leemans R (2006) Technology development and climate change as drivers of future agricultural land use. In: Brouwer F, McCarl BA (Eds.), Agriculture and Climate Beyond 2015 Environ-ment and Policy 46, pp. 33–51.

FAO (2011) State of the World's forests. Forestry Department, Rome

Foley JA et al (2005) Global Consequences of Land Use Science 309: 570–574. doi:10.1126/science.1111772

Freitas SR, Hawbaker TJ, Metzger JP (2010) Effects of roads topography, and land use on forest cover dynamics in the brazilian atlantic forest. For Ecol Manage 259:410–417

Fu BJ et al (2006) Temporal change in land use and its relationship to slope degree and soil type in a small catchment on the loess plateau of China. Catena 65:41–48

Fung T, So LLH, Chen Y, Shi P, Wang J (2008) Analysis of green space in Chongqing and Nanjing, cities of China with ASTER images using object oriented image classification and landscape metric analysis international. Journal of Remote Sensing 29:7159–7180. doi:10.1080/01431160802199868

GBO3 (2010) Secretariat of the Convention on Biological Diversity. Global Biodiversity Outlook 3—Executive Summary, Montreal

Geomatica (2013) Atmospheric correction (with ATCOR)

Ghimire B, Rogan J, Miller J (2010) Contextual land-cover classification: incorporating spatial dependence in land-cover classification models using random forests and the Getis statistic. Remote Sensing Letters 1:45–54. doi:10.1080/01431160903252327

Gislason PO, Benediktsson JA, Sveinsson JR (2006) Random forests for land cover classification. Pattern Recogn Lett 27:294–300. doi:10.1016/j.patrec.2005.08.011

Haines-Young R (2009) Land use and biodiversity relationships. Land Use Policy 26(1):178–186

Horskins K, Mather PB, Wilson JC (2006) Corridors and connectivity: when use and function do not equate. Landsc Ecol 21(5):641–655

Hua WJ, Chen HS (2013) Impacts of regional-scale land use/land cover change on diurnal temperature range. Adv Clim Chang Res 4:166–172. doi:10.3724/SP.J.1248.2013.166

Johnson BA (2013) High-resolution urban land-cover classification using a competitive multi-scale object-based approach. Remote Sensing Letters 4(2):131–140

Kampouraki M, Wood GA, Brewer TR (2008) Opportunities and limitations of object based image analysis for detecting urban impervious and vegetated surfaces using true-colour aerial photography. In: Blaschke T, Lang S, Hay G (eds) Object-based image analysis. Lecture notes in Geoinformation and cartography. Springer, Berlin Heidelberg, pp 555–569. doi:10.1007/978-3-540-77058-9_30

Kang JH, Lee SW, Cho KH, Ki SJ, Cha SM, Kim JH (2010) Linking land-use type and stream water quality using spatial data of fecal indicator bacteria and heavy metals in the Yeongsan river basin. Water Res 44:4143–4157. doi:10.1016/j.watres.2010.05.009

Keshtkar H, Voigt W (2016a) A spatiotemporal analysis of landscape change using an integrated Markov chain and cellular automata models model. Earth Syst Environ 2:1–13. doi:10.1007/s40808-015-0068-4

Keshtkar H, Voigt W (2016b) Potential impacts of climate and landscape fragmentation changes on plant distributions: coupling multi-temporal satellite imagery with GIS-based cellular automata model. Ecological Informatics 32:145–155. doi:10.1016/j.ecoinf.2016.02.002

Keshtkar HR, Azarnivand H, Arzani H, Alavipanah SK, Mellati F (2013) Land cover classification using IRS-1D data and a decision tree classifier. Desert 17:137–146

Kuemmerle T, Chaskovskyy O, Knorn J, Radeloff VC, Kruhlov I, Keeton WS, Hostert P (2009) Forest cover change and illegal logging in the Ukrainian Carpathians in the transition period from 1988 to 2007. Remote Sens Environ 113:1194–1207. doi:10.1016/j.rse.2009.02.006

Lambin EF, Geist HJ (2003) Regional differences in tropical deforestation. Environment: Science and Policy for Sustainable Development 45:22–36. doi:10.1080/00139157.2003.10544695

Lambin EF, Meyfroidt P (2011) Global land use change, economic globalization, and the looming land scarcity Proceedings of the National Academy of Sciences 108:3465–3472 doi:10.1073/pnas.1100480108

Lawrence PJ et al (2012) Simulating the biogeochemical and Biogeophysical impacts of transient land cover change and wood harvest in the community climate system model (CCSM4) from 1850 to 2100. J Clim 25: 3071–3095. doi:10.1175/JCLI-D-11-00256.1

Le Houérou HN (1996) Climate change, drought and desertification. J Arid Environ 34:133–185. doi:10.1006/jare.1996.0099

Li S, Gu S, Tan X, Zhang Q (2009) Water quality in the upper Han River basin, China: the impacts of land use/land cover in riparian buffer zone. J Hazard Mater 165:317–324. doi:10.1016/j.jhazmat.2008.09.123

Licciardi G et al (2009) Decision fusion for the classification of hyperspectral data: outcome of the 2008 GRS-S data fusion contest geoscience and remote sensing. IEEE Transactions on 47:3857–3865. doi:10.1109/TGRS.2009.2029340

Lind B, Stein S, Kärcher A, Klein M (2009) Where have all the flowers gone? Grünland im Umbruch. German Federal Agency for Nature Conservation (BfN), Bonn

Liu D, Xia F (2010) Assessing object-based classification: advantages and limitations. Remote Sensing Letters 1:187–194. doi:10.1080/01431161003743173

Loeb C (2006) Planning reunification: the planning history of the fall of the Berlin Wall. Plan Perspect 21(1):67–87

Long HL, Wu XQ, Wang WJ, Dong GH (2008) Analysis of urban-rural land-use change during 1995-2006 and its policy dimensional driving forces in Chongqing. China Sensors 8:681–699

Loveland TR, Belward AS (1997) The IGBP-DIS global 1 km land cover data set, DISCover: first results. Int J Remote Sens 18:3289–3295. doi:10.1080/014311697217099

Lu D, Weng Q (2007) A survey of image classification methods and techniques for improving classification performance. Int J Remote Sens 28:823–870. doi:10.1080/01431160600746456

Manandhar R, Odeh I, Ancev T (2009) Improving the accuracy of land use and land cover classification of Landsat data using post-classification enhancement. Remote Sens 1:330

Möller M, Lymburner L, Volk M (2007) The comparison index: a tool for assessing the accuracy of image segmentation. Int J Appl Earth Obs Geoinf 9:311–321. doi:10.1016/j.jag.2006.10.002

Myint SW, Gober P, Brazel A, Grossman-Clarke S, Weng Q (2011) Per-pixel vs. object-based classification of urban land cover extraction using high spatial resolution imagery. Remote Sens Environ 115:1145–1161. doi:10.1016/j.rse.2010.12.017

Oke TR (1987) Boundary layer climates, 2nd edn. Methuen & Co. Ltd., New York, NY

Otukei JR, Blaschke T (2010) Land cover change assessment using decision trees, support vector machines and maximum likelihood classification algorithms. Int J Appl Earth Obs Geoinf 12:S27–S31. doi:10.1016/j.jag.2009.11.002

Pal M, Mather PM (2005) Support vector machines for classification in remote sensing. Int J Remote Sens 26:1007–1011. doi:10.1080/01431160512331314083

Petropoulos GP, Vadrevu KP, Xanthopoulos G, Karantounias G, Scholze M (2010) A comparison of spectral angle mapper and artificial neural network classifiers combined with Landsat TM imagery analysis for obtaining burnt area mapping. Sensors (Basel, Switzerland) 10:1967–1985. doi:10.3390/s100301967

Poschlod P, Bakker JP, Kahmen S (2005) Changing land use and its impact on biodiversity. Basic and Applied Ecology 6:93–98. doi:10.1016/j.baae.2004.12.001

Pu R, Landry S, Yu Q (2011) Object-based urban detailed land cover classification with high spatial resolution IKONOS imagery. Int J Remote Sens 32:3285–3308. doi:10.1080/01431161003745657

Qian Y, Zhou W, Yan J, Li W, Han L (2014) Comparing machine learning classifiers for object-based land cover classification using very high resolution imagery. Remote Sens 7:153

Quinlan JR (1987) Simplifying decision trees. Int J Man-Mach Stud 27:221–234. doi:10.1016/s0020-7373(87)80053-6

R Core Team (2013) R: A language and environment for statistical computing. R foundation forstatistical computing. Vienna, Austria. http://www.R-project.org/

Riecken U, Finck P, Raths U, Schröder E, Ssymank A (2008) Die Gefährdung der Biotoptypen in Deutschland Aktueller Stand nach Vorlage der 2 Fassung der Roten Liste Natursch. Biol Vielf 2008:189–194

Robinson DJ, Redding NJ, Crisp DJ (2002) Implementation of a fast algorithm for segmenting SAR imagery. Defense Science and Technology Organization, Australia

Rodriguez-Galiano VF, Chica-Rivas M (2012) Evaluation of different machine learning methods for land cover mapping of a Mediterranean area using multi-seasonal Landsat images and digital terrain models. International Journal of Digital Earth 7:492–509. doi:10.1080/17538947.2012.748848

Settel A (1946) A year of Potsdam: the German economy since the surrender. Lithographed by the Adjutant General. OMGUS, USA, p 217

Shrestha DP, Zinck JA (2001) Land use classification in mountainous areas: integration of image processing, digital elevation data and field knowledge (application to Nepal). Int J Appl Earth Obs Geoinf 3:78–85

Siehoff S, Lennartz G, Heilburg IC, Roß-Nickoll M, Ratte HT, Preuss TG (2011) Process-based modeling of grassland dynamics built on ecological indicator values for land use. Ecol Model 222:3854–3868. doi:10.1016/j.ecolmodel.2011.10.003

Stuckens J, Coppin PR, Bauer ME (2000) Integrating contextual information with per-pixel classification for improved land cover classification. Remote Sens Environ 71:282–296. doi:10.1016/S0034-4257(99)00083-8

Szantoi Z, Escobedo F, Abd-Elrahman A, Smith S, Pearlstine L (2013) Analyzing fine-scale wetland composition using high resolution imagery and texture features. Int J Appl Earth Obs 23:204–212

Szantoi Z et al (2015) Classifying spatially heterogeneous wetland communities using machine learning algorithms and spectral and textural features. Environ Monit Assess 187:262. doi:10.1007/s10661-015-4426-5

Therneau T, Atkinson E (1997) An introduction to recursive partitioning using the RPART routines. Mayo Clinic, Rochester, MN

Tian F, Yang L, Lv F, Zhou P (2009) Predicting liquid chromatographic retention times of peptides from the *Drosophila melanogaster* proteome by machine learning approaches. Anal Chim Acta 644:10–16. doi:10.1016/j.aca.2009.04.010

Tölle A (2010) Urban identity policies in berlin: from critical reconstruction to reconstructing the wall. Cities 27:348–357

Van Coillie FMB, Verbeke LPC, De Wulf RR (2007) Feature selection by genetic algorithms in object-based classification of IKONOS imagery for forest mapping in Flanders. Belgium Remote Sensing of Environment 110:476–487. doi:10.1016/j.rse.2007.03.020

Vapnik VN (1995) The nature of statistical learning theory. Springer

Waske B, van der Linden S, Oldenburg C, Jakimow B, Rabe A, Hostert P (2012) imageRF – a user-oriented implementation for remote sensing image analysis with random forests. Environ Model Softw 35:192–193. doi:10.1016/j.envsoft.2012.01.014

Wen L et al (2013) Effect of degradation intensity on grassland ecosystem services in the alpine region of Qinghai-Tibetan plateau. China PLos ONE 8:e58432. doi:10.1371/journal.pone.0058432

Wu X, Shen Z, Liu R, Ding X (2008) Land use/cover dynamics in response to changes in environmental and socio-political forces in the upper reaches of the Yangtze River. China Sensors 8:8104–8122. doi:10.3390/s8128104

Yu Q, Gong P, Clinton N, Biging G, Kelly M, Schirokauer D (2006) Objectbased detailed vegetation classification with airborne high spatial resolution remote sensing imagery. Photogrammetric Engineering and Remote Sensing 72(7):799–811

Yuan F, Sawaya KE, Loeffelholz BC, Bauer ME (2005) Land cover classification and change analysis of the twin cities (Minnesota) metropolitan area by multitemporal Landsat remote sensing. Remote Sens Environ 98:317–328. doi:10.1016/j.rse.2005.08.006

Zhao Y et al (2014) Effects of topography on status and changes in land-cover patterns. Chongqing City, China Landscape Ecol Eng 10:125–135. doi:10.1007/s11355-011-0155-2